Contrasting climate change impact on river flows from high-altitude catchments in the Himalayan and Andes Mountains

Silvan Ragettli[a,1], Walter W. Immerzeel[b], and Francesca Pellicciotti[c]

[a]Institute of Environmental Engineering, ETH Zurich, 8093 Zurich, Switzerland; [b]Department of Physical Geography, Utrecht University, 3508 TC Utrecht, The Netherlands; and [c]Department of Geography, Northumbria University, Newcastle upon Tyne NE1 8ST, United Kingdom

Edited by Andrea Rinaldo, Laboratory of Ecohydrology, Ecole Polytechnique Federale Lausanne, Lausanne, Switzerland, and approved June 21, 2016 (received for review April 26, 2016)

Mountain ranges are the world's natural water towers and provide water resources for millions of people. However, their hydrological balance and possible future changes in river flow remain poorly understood because of high meteorological variability, physical inaccessibility, and the complex interplay between climate, cryosphere, and hydrological processes. Here, we use a state-of-the art glacio-hydrological model informed by data from high-altitude observations and the latest climate change scenarios to quantify the climate change impact on water resources of two contrasting catchments vulnerable to changes in the cryosphere. The two study catchments are located in the Central Andes of Chile and in the Nepalese Himalaya in close vicinity of densely populated areas. Although both sites reveal a strong decrease in glacier area, they show a remarkably different hydrological response to projected climate change. In the Juncal catchment in Chile, runoff is likely to sharply decrease in the future and the runoff seasonality is sensitive to projected climatic changes. In the Langtang catchment in Nepal, future water availability is on the rise for decades to come with limited shifts between seasons. Owing to the high spatiotemporal resolution of the simulations and process complexity included in the modeling, the response times and the mechanisms underlying the variations in glacier area and river flow can be well constrained. The projections indicate that climate change adaptation in Central Chile should focus on dealing with a reduction in water availability, whereas in Nepal preparedness for flood extremes should be the policy priority.

river flow | glaciers | climate change | high-altitude water cycle | hydrological modeling

Glaciers and seasonal snow cover change their water storage capacity under a warming climate. When glacier mass balances are negative, glaciers contribute additional water to rivers. However, negative mass balances lead to a reduction in glacier volume and area, which eventually reduces the total meltwater from glaciers. A warming climate may therefore lead to either rising or decreasing river flows, depending on the state of glacier retreat (1). Due to variability in glacier characteristics and differences in climate, high-altitude regions respond differently to climatic changes across the world (2). Factors that potentially retard glacier response to global warming are the presence of thick, insulating layers of supraglacial debris (3), topographic shading due to extreme topography (4), or steep and large headwalls, which cause the glacier's response to be dictated by local avalanche processes (5). Factors that increase melt rates are decreases in albedo due to mineral dust and black carbon depositions (6) and prolonged melting seasons (7). Furthermore, glacier sensitivity to global warming depends strongly on precipitation seasonality (7). Temperature increase leads to a change in precipitation phase over summer accumulation-type glaciers (such as in the Central and Eastern Himalaya), whereas this is not necessarily the case with winter precipitation. The rate of change of net glacier mass loss depends also on initial glacier hypsometry (8): glacier mass balances become very negative if the equilibrium line altitude (ELA) rises above the elevations where most initial glacier area is located. This seems the case currently over most of Central Europe and at low latitudes, whereas in Alaska and High Mountain Asia a large portion of glacier area is above the current-day ELA (8). Given the multitude of control factors, often acting at relatively small scales, current projections of global glacier change models do not constrain the mechanisms underlying the variations in river flow from high-altitude catchments well (2, 8, 9). It is therefore uncertain if such models can correctly capture the response times and the magnitudes of future changes. Modeling studies at a high spatiotemporal resolution and degree of process complexity are crucial to assess the impact of climate change on the hydrological balance of high-altitude catchments and to refine the projections of the coarser-scale models (10, 11).

Here, we compare the impact of climate change on the magnitude and timing of catchment runoff for two climatically contrasting high-altitude areas in the Himalayan and Andean Mountains with a model configuration that substantially exceeds the spatiotemporal resolutions and degree of complexity of previous intercontinental comparative studies (2, 8, 9). Whereas global-scale modeling studies work with routines and parameters that are assumed to be generally valid, the simulations presented here are based on model setups that have been thoroughly evaluated in three companion papers (12–14) to correctly reproduce present observed catchment runoff, meteorological processes, snow cover variability, and glacier mass balances. Model construction and calibration benefited from extensive short-term field campaigns, which allowed overcoming the problem of data scarcity typical of poorly accessible high-altitude regions.

We make projections of 21st century runoff and glacier changes using the state-of-the art glacio-hydrological model TOPKAPI-ETH

Significance

Changes in the hydrology of high-altitude catchments may have major consequences for downstream water supply. Based on model projections with a higher spatiotemporal resolution and degree of process complexity than any previous intercontinental comparative study, we show that the impacts of climate change cannot be generalized. These impacts range from a high climatic sensitivity, decreasing runoff, and significant seasonal changes in the Central Andes of Chile to increasing future runoff, limited seasonal shifts, but increases in peak flows in the Nepalese Himalaya. This study constrains uncertainty about response times and mechanisms controlling glacier and runoff response to climate and sets a benchmark for process-based modeling of the climate change impact on the hydrology of high-altitude catchments.

Author contributions: F.P. designed research; S.R., W.W.I., and F.P. performed research; S.R. contributed new reagents/analytic tools; S.R. analyzed data; and S.R., W.W.I., and F.P. wrote the paper.

The authors declare no conflict of interest.

This article is a PNAS Direct Submission.

Freely available online through the PNAS open access option.

[1]To whom correspondence should be addressed. Email: ragettli@ifu.baug.ethz.ch.

This article contains supporting information online at www.pnas.org/lookup/suppl/doi:10.1073/pnas.1606526113/-/DCSupplemental.

(12–15), the newest climate change scenarios (*SI Appendix*, Table S2), and performing simulations at a spatial resolution of 100 m and hourly time steps. The high spatial resolution ensures that processes acting at relatively small scales such as gravitational snow redistribution or topographic shading are taken into account. The high temporal resolution allows to reproduce the strong subdaily variability of melt rates and to accurately determine the altitude of the freezing level and its diurnal cycles. Short-term variability of temperature has a large effect on the duration of melting episodes (16). Simulations provided here allow for an examination of future runoff extremes, which have been little investigated to date in the Himalayan (17) and Andean Mountains.

Uncertainty in model projections is quantified by taking into account a large subset of climate models, representative of the uncertainty range of the original Coupled Model Intercomparison Project Phase 5 (CMIP5) ensemble. We analyze two main scenarios [representative concentration pathways (RCPs)] that may lead to a radiative forcing of 4.5 W/m^2 (RCP45) and 8.5 W/m^2 (RCP85) in 2100. The two RCPs chosen are the climate scenarios for which the largest number of climate models are available. For each RCP and each watershed, 12 global climate models (GCMs) are considered and stochastically downscaled to the location of the study catchments. The stochastic approach allows accounting for the uncertainty due to the natural variability of the climate system (15, 18) and is particularly useful for an analysis of extremes because the multiple model runs for each GCM-RCP combination allow a statistical assessment of peak events that occur with a low frequency.

Two study catchments (the Juncal catchment in the Central Andes of Chile and the Upper Langtang catchment in the Nepalese Himalaya) are selected for their proximity to densely populated areas (Fig. 1) and their representativeness in terms of meteorology, hydrology, and glacier processes for the same elevations in the two large climatic regions (*SI Appendix*, Fig. S2). The Central Andes of Chile are among the most vulnerable regions to changes in the cryosphere, because meltwater from glaciers and snow is critical to maintain river flows during the dry summers (10, 19) and because of increasing water demand in the downstream regions (20). Large glaciers exist due to high accumulation area ratios in El Niño years and local effects like topographic shading and accumulation through avalanches and wind (19, 21, 22). In the Nepalese Himalaya, glaciers influence the hydrology of the Upper Ganges Basin (17), which is marked by intense competition on water resources because of high population density and extensive irrigation needs (23). However, more than 70% of the annual precipitation occurs during the warmest period of the year, which dampens the relative contribution of snowmelt and ice melt on the annual water yield (12). The large glaciers with low-reaching tongues in this climate are characterized by heavy debris cover that protects them from melting (12, 24).

Results

The temperature projections reveal similar warming trends for the Langtang and Juncal region (Fig. 1 *A* and *B*). Between 2010 and 2100, mean temperatures are projected to increase between 1.1 and 3.4 °C for RCP45 and between 3.4 and 7.2 °C for RCP85 for the two regions, depending on the GCM. Precipitation projections show a negative trend for the Central Andes of Chile and a contrasting positive trend for the Nepalese Himalaya, and in both cases those trends are pronounced for the RCP85 scenario. However, the uncertainty in precipitation projections is generally large, in particular for Central Chile, where projected end-of-century precipitation changes vary between −50% and +15% in comparison with the beginning of the century (Fig. 1*A*).

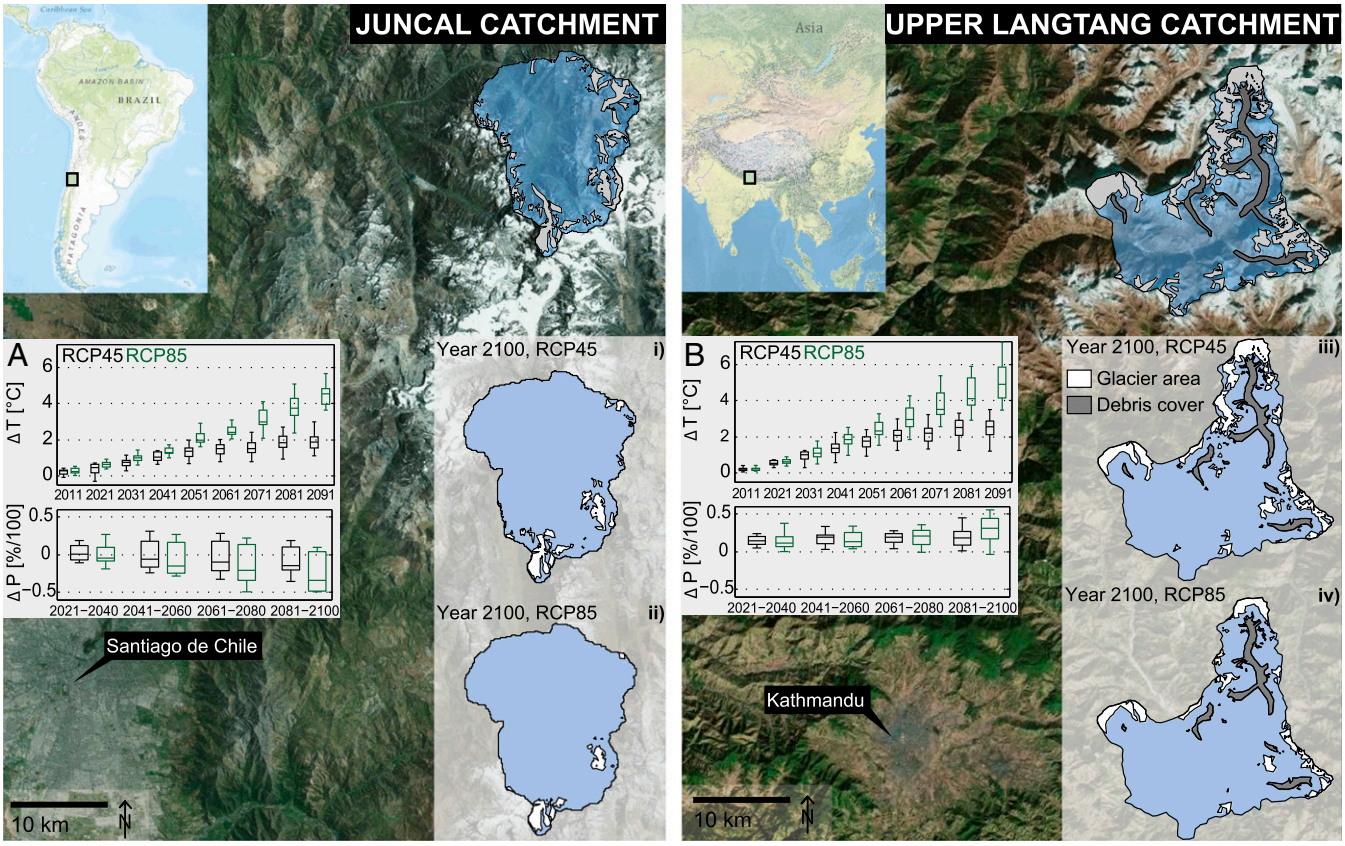

Fig. 1. Study catchments and glacier and debris-covered area at the beginning of the century. (*A* and *B*) The boxes showing the 25th, 50th, and 75th percentile of the GCM ensemble projections indicate relative changes in projected decadal mean annual precipitation and temperature with respect to the reference period (2001–2010). (*i–iv*) Ensemble-median projected glacier area (RCP45 and RCP85) by the year 2100.

River Flow Projections. The Upper Langtang catchment exhibits increasing runoff in the first half of the 21st century for all climate scenarios (between +15% and +70% in comparison with 2001–2010; Fig. 2). Under RCP45 conditions, the simulations indicate a possible runoff decrease after the peaking in 2051–2060. Under RCP85 conditions, Langtang River runoff remains relatively stable during the second half of the 21st century, but with an increasing GCM uncertainty. In contrast to the projections for the Nepalese Himalaya, decreasing water availability is a plausible scenario for the Central Andes of Chile. The multimodel median projections for the Juncal catchment indicate stable runoff volumes until 2021–2030 and then a steadily decreasing trend. Multimodel median runoff under RCP45 conditions declines by 40% between 2001–2010 and 2091–2100, and by 62% under RCP85 conditions. Although the described trends are consistent across GCMs for the Upper Langtang catchment, the runoff trends projected for the Juncal catchment differ between climate models. Here, the projections by 5 out of 12 climate models lead to a stable runoff response until the end of the century rather than a steady decline.

Fate of Glaciers. Both catchments respond with a clear decreasing trend in glacier area to the changes in climate. Multimodel median results indicate 53% (RCP45) or 70% (RCP85) glacier area loss in the Juncal region between 2001–2010 and 2091–2100 (Fig. 3). For the same period, the simulations indicate a decrease in glacierized area by 35% (RCP45) or 55% (RCP85) for the Langtang region (Fig. 3). Debris-covered glacier area (representing 27% of the total glacier area in Langtang) is less sensitive to the changes in climate and decreases only by 25% (RCP45) or 33% (RCP85) until the end of the century. It is typical of heavily debris-covered glaciers with stagnant low-gradient termini that fronts are more stable (25). High air temperatures prevailing on the low-reaching tongues and enhanced melting on exposed ice cliffs and beneath supraglacial lakes can substantially mitigate the shielding effect of supraglacial debris (26–29). However, in the Langtang region, melt rates of debris-covered ice are much lower than of non–debris-covered ice (12). In the long run, this leads to glacier tongues that are disconnected from the accumulation areas (Fig. 1 *iii* and *iv* and *SI Appendix*, Fig. S12).

Glacier Contributions to River Flow. Ice melt from glaciers represents roughly one-third of total simulated streamflow during the reference period (2001–2010) in Langtang, and one-fifth in Juncal (Fig. 2). We show that total ice melt is on a rising limb in Langtang at least until 2041–2050 and starts to decrease again after 2051–2060 (Fig. 3). These results confirm the findings by a previous modeling study (30). In Juncal, however, total ice melt was already beyond its tipping point at the beginning of the 21st century according to our simulations. This contrasting response to climate warming can be explained by differences in the elevation distribution of the glaciers in the two regions. In Juncal, many glaciers are melting up to the highest elevations already during the reference period. Increasing melt rates due to higher air temperatures cannot compensate the continuous loss of glacier area. In the Langtang catchment, large sections of the glaciers at high elevations are currently not exposed to melt, but will be in the future, and thus compensate for the loss of glacier area at lower elevations (*SI Appendix*, Fig. S11). Total glacier area contributing to melt in Langtang peaks in 2051–2060 (Fig. 3 *B* and *C*). In Juncal, glacier area contributing to melt decreases steadily (Fig. 3 *E* and *F*).

The decline in total ice melt in Langtang after 2051–2060 is compensated by a very pronounced increase in total rainfall (*SI Appendix*, Fig. S10*C*), which is due to the projected increase in precipitation by most climate models. During the second half of the century, the contribution of ice melt to total water inputs decreases by 10%, whereas the contribution of rainfall increases by 10% according to median projections (Fig. 2). Other studies have argued that, in a monsoon-dominated climate, the glacier contribution to water availability is minor (2, 31). Our results confirm that the effect of runoff decrease due to glacier decline is dampened by high relative (increasing) contributions of rain. However, if the contributions of glaciers in the Langtang catchment remained constant and were not decreasing after midcentury (Fig. 3), runoff would further increase rather than decrease or remain constant (Fig. 2 *A* and *B*). In the Juncal catchment, the decline in total ice melt until the end of the century (Fig. 3*D*) explains 30–40% of annual runoff declines (Fig. 2 *C* and *D*).

Future Runoff Seasonality. The changes in the hydrology of the Juncal catchment are such that peak runoff during the austral summer disappears gradually (Fig. 4). By the end of the century, the differences between winter, spring, and summer runoff become very small (under RCP85 conditions). The climate projections by five GCMs (RCP85) lead to an earlier peak runoff shifted by 2–3 mo, whereas the simulations associated to a majority of climate models (both RCP45 and RCP85) indicate an anticipation of the seasonal runoff peak by 1 mo. The shifts in the seasonality can be explained by earlier snowmelt onset and a change of phase from liquid to solid precipitation. Total rainfall amounts will likely increase (*SI Appendix*, Fig. S10*G*)—despite mostly decreasing precipitation. In the Upper Langtang catchment, on the other hand, the changes in climate lead to almost no changes in runoff seasonality (Fig. 4), because the timing of the monsoon period and of the main melting season essentially remains unaffected by climate change. However, the hydrological regime changes to a more rainfall-dominated regime, which results in a faster transition of precipitation to runoff and a higher susceptibility to peak flows.

Future Runoff Extremes. Our simulations indicate a substantial increase in the magnitude of peak runoff events for the Upper Langtang catchment, particularly under RCP85 conditions (Fig. 5*A* and *SI Appendix*, Figs. S8 and S9). The model runs indicate increasing annual maximum daily flows with increasing peak flows

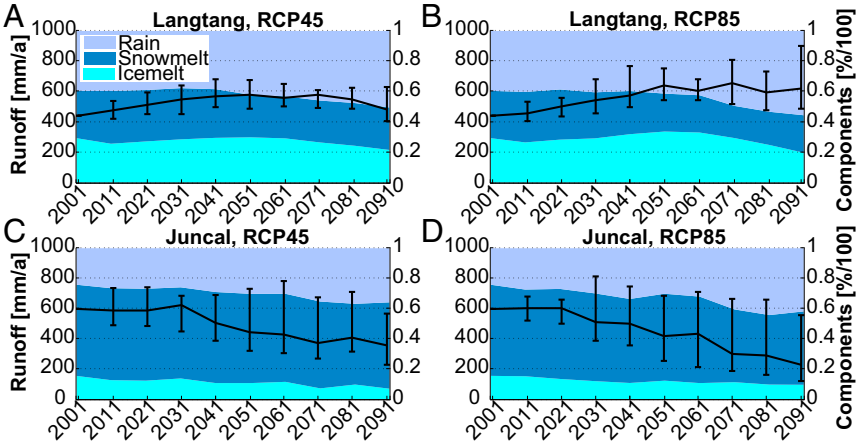

Fig. 2. Future catchment runoff and composition of total water input. The figure shows the median of all simulations for each decade, RCP, and study area (*A* and *B*: Upper Langtang catchment; *C* and *D*: Juncal catchment). The error bars represent the 80% confidence interval about the climate model ensemble.

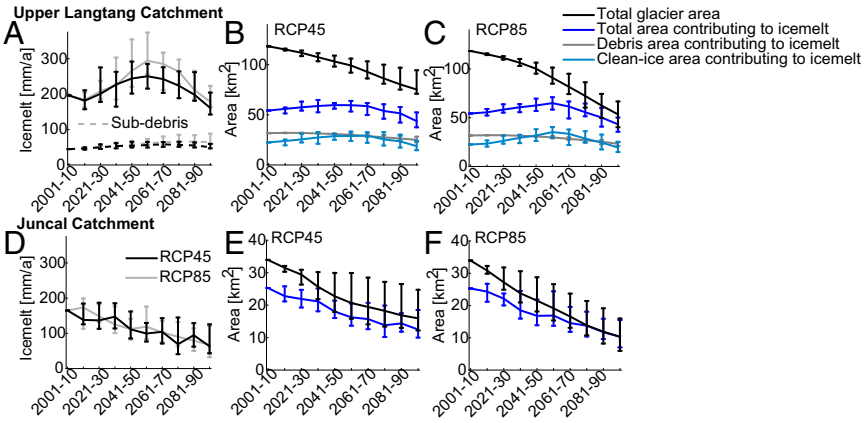

Fig. 3. Future evolution of ice melt contribution to runoff, future glacier area, and glacier area contributing to ice melt. The lines show the median of all simulations for each decade, RCP, and study area (*A*–*C*: Upper Langtang catchment; *D*–*F*: Juncal catchment). Subdebris ice melt (*A*) is a component of total ice melt in the Upper Langtang catchment. The debris-covered glacier area and non–debris-covered glacier area contributing to ice melt are shown separately (*B* and *C*). The bars represent the 80% confidence interval about the climate model ensemble (also shown for debris area contributing to ice melt but too close to the line to see).

especially during the postmonsoon season. Annual maximum daily flows with recurrence intervals of 10 y are projected to increase by 100% until the end of the century (Fig. 5*A*). The higher peak flows can be related to precipitation state changes from solid to liquid during extreme precipitation events related to cyclonic disturbances (32, 33). This result is therefore not affected by the common limitations of climate models and bias correction techniques in predicting new precipitation extremes outside empirical ranges (34), or by the large uncertainties in precipitation projections. In Juncal, simulated future annual peak flows remain approximately constant in magnitude (Fig. 5*B*), due to shifts in seasonal flows (Fig. 4 and *SI Appendix*, Fig. S9) despite total annual runoff decreases (Fig. 2). For future dry years (cumulative probability of annual runoff less than 50%), the model projects no reduction in water availability in comparison with the present in Langtang, but 10–30% stronger decreases than for average years in Juncal (*SI Appendix*, Fig. S8).

Discussion

Our findings point to the necessity of identifying coping strategies to a reduction in water availability in the Central Andes of Chile. All simulations for the Juncal region indicate a significant decrease in summer runoff until the end of the century, and more than 90% of the runs a decrease in total annual runoff. In contrast to the Central Andes of Chile, there are no signs of decreasing water availability in the Nepalese Himalaya. Here, future research will have to focus on changes in the return periods of water-related natural hazards and assess the downstream impact of strong increases in postmonsoon peak flows from high elevation catchments as projected by our study.

Global glacier change models (2, 8, 9) project strong glacier area and volume decreases until the end of the century for the Southern Himalaya (e.g., ref. 8, RCP45, −70% glacier area by the year 2100), which also leads to projections of continuously decreasing glacier runoff (2). However, such projections are representative of very large regions, and therefore the comparability with the outputs of the present study is limited. However, both Juncal and Langtang are located near urban centers and therefore have a high interest for stakeholders of water resources. Here, large-scale studies are not suitable to inform policy making regarding climate change adaptation, given also the large differences between our projections and the regionally averaged outputs of global models. Apart from different glacier ensembles considered, the much stronger glacier retreat projections by global models for the Southern Himalaya in comparison with our study could be explained by the nonconsideration of the insulating effect of supraglacial debris and/or the application of simple temperature index models, which tend to be oversensitive to temperature fluctuations (35).

There are also important differences in the outputs of previous detailed climate change impact modeling studies focusing on the Upper Langtang catchment. Water released by glaciers plays a more important role for future runoff from the Upper Langtang catchment than suggested by two previous studies (30, 36), and as a consequence future runoff is not entirely governed by the future precipitation trend. Our study projects stagnating (RCP85) or slightly decreasing (RCP45) runoff after midcentury, whereas refs. 30 and 36 indicate a consistent increase throughout the 21st century (both RCPs). Here, differences in model structure and between calibration strategies explain the differences in model projections. The consideration of a separate term for shortwave radiation in the melt algorithms used by

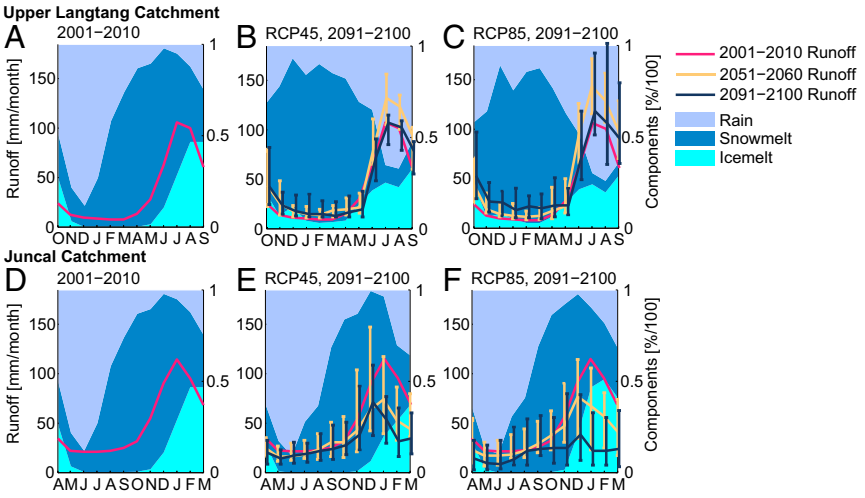

Fig. 4. Simulated seasonal runoff cycles and water input composition. The median results of all simulations are represented. Error bars represent the 80% confidence interval of the climate model uncertainty. The composition of water inputs is shown for the reference period 2001–2010 (*A* and *D*), for the period 2091–2100 and RCP45 projections (*B* and *E*), and for the period 2091–2100 and RCP85 projections (*C* and *F*). Solid lines represent the median of all simulations for the reference period (2001–2010) and two future periods (2051–2060 and 2091–2100).

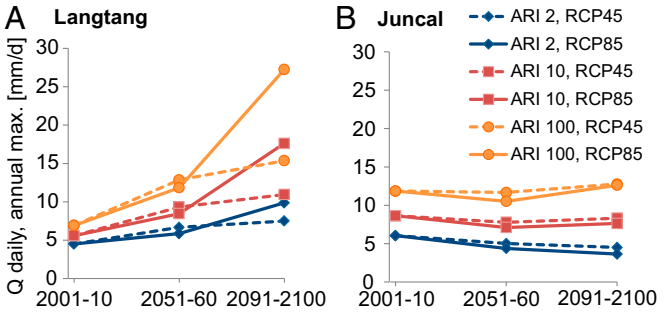

Fig. 5. Simulated annual maximum daily runoff corresponding to average recurrence intervals of 2 y (ARI 2), 10 y (ARI 10), and 100 y (ARI 100) for both RCPs (RCP45 and RCP85) and study areas (*A*: Upper Langtang catchment; *B*: Juncal catchment). The figure shows the median outputs of the stochastic runs for the reference period (2001–2010) and for two future decades (2051–2060 and 2091–2100).

this study assures that the relationships between air temperature and melt are robust in time and thus suitable for long-term modeling (35). The higher spatiotemporal resolution and degree of process complexity allows representing the heterogeneous snowmelt and ice melt patterns controlled by solar radiation or supraglacial debris. Glacio-hydrological models in high-altitude regions are also particularly sensitive to assumptions about temperature gradients (refs. 12–15; *SI Appendix*, Fig. S5). While in this study temperature gradients are based on measured detailed information about air temperature distribution, previous catchment scale models in the region use substantially different approaches to determine temperature lapse rates. Parameterizations were obtained through model calibration (30, 36), which may lead to equifinality and error compensation (37). Other studies use reanalysis products (17, 38) or remotely sensed data (39), which are, however, more uncertain data sources and available only at relatively coarse resolutions.

A distributed model characterized by a high degree of complexity such as TOPKAPI-ETH requires a good knowledge of internal states to correctly represent the basin-internal dynamics (40). We therefore highlight the utility of in situ data to inform glacio-hydrological models for climate change impact assessments. We argue that more such data collection efforts are required for climate change impact assessment across climates and regions. A smart integration of field-based studies with the catchment scale at key basins in the world has great potential and can reveal the full magnitude of the impacts of climate change on mountain water resources.

Materials and Methods

Main Model. We use a fully distributed, high-resolution (100 m, hourly time step) glacio-hydrological model, TOPKAPI-ETH (12–15), in two glacierized catchments of the Himalaya and the Andes. The model simulates all major hydrological and glaciological processes at the watershed scale. As input variables, the model requires distributed fields of air temperature, precipitation, and cloud transmittance factors.

Snowmelt and Ice Melt. Snow and ice ablation is modeled with an enhanced temperature index (ETI) approach, where melt in each grid cell is the sum of a temperature-dependent term and a shortwave radiation-dependent term (41). The approach considers therefore the fully distributed shortwave radiation balance, which is calculated from the position of the sun relative to the considered grid cell, topographic shading, cloudiness, and surface albedo. Snow albedo decreases over time if air temperatures are above the melting point (42), and constant ice albedo is used by the ETI to calculate ice melt once snow is depleted.

Supraglacial Debris. Subdebris ice melt is calculated using a debris–ETI approach, where ablation rates decrease in function of debris thickness. Debris thickness is reconstructed by an inverse Ostrem approach (12), relating observed surface elevation change rates to debris thicknesses according to an Ostrem curve established using a debris–energy balance model (43). Stagnant glacier area is chosen for this purpose to limit the error due to ice thickening in response to compressive flow regimes. Surface elevation changes are obtained from differencing two high-resolution digital elevation models from unmanned aerial vehicle surveys (44). Debris thicknesses of areas without information about surface elevation changes are parameterized based on the position relative to the snout and the presence of supraglacial lakes identified from Landsat ETM+ multispectral data (12). The spatial density of supraglacial lakes is used as a proxy for spatial variations in debris thickness because these features (in combination with supraglacial cliffs whose presence correlates with the presence of lakes) have been shown to greatly influence downwasting rates of debris-covered glacier ice (27, 28, 45).

Avalanching. Gravitational snow redistribution is taken into account with a mass conservation algorithm based on slope-dependent maximum snow holding depths (46). If the threshold depth is exceeded, snow is moved to the next model grid cell downward.

Glacier Dynamics. We assume a linear increase of glacier thinning rates below a given threshold elevation and a constant ice thickness above, which guarantees that ice accumulated above the ELA is redistributed to lower elevations and that declines in glacier area are delayed by flow dynamics (47). The approach is mass conserving, which implies that thinning rates depend on annually accumulated ice volumes. Snow-to-ice conversion takes place where snow remains on a glacier for longer than a year. Ice depths remain constant if the ice mass balance of a given glacier for a given year is zero. Initial ice thicknesses are estimated using the model GlabTop2 (48), which is essentially a slope-dependent ice thickness estimation approach. The glacier dynamics algorithm is executed once a year at the end of each hydrological year.

Routing, Groundwater, and Evapotranspiration. Reference evapotranspiration (RET) depends on incoming shortwave radiation, albedo, and air temperature. Vegetation coefficients determine the ratio between potential evapotranspiration and RET. Actual evapotranspiration depends on available soil moisture content within a superficial soil layer calculated internally by TOPKAPI-ETH. A second soil layer accounts for runoff originating from percolation to deeper soil and into fractured bedrock. Water routing in is based on the kinematic wave concept, whereby subsurface flow, overland flow due to infiltration or saturation excess, and channel flow are represented by nonlinear reservoir differential equations (49).

GCM Data. A subset of 12 GCMs (*SI Appendix*, Table S2) is selected for the RCP45 and RCP85 scenarios from the latest climate model ensemble generated for the Intergovernmental Panel on Climate Change fifth assessment report provided through CMIP5. In order for the subset to be representative of the uncertainty range of the original CMIP5 ensemble, the selected GCMs are sampled randomly from clusters of multivariate characteristics regarding the changes in temperature and precipitation projected for both the Andes and the Himalaya (*SI Appendix*, Fig. S2). We use daily precipitation and monthly temperature climate model outputs.

GCM Downscaling. We use a stochastic approach to downscale the climate models (15, 18) to generate hourly input time series until 2100. Temperature and precipitation data are downscaled to the location of the closest permanent meteorological station in each region. Each station provides at least 9 y of data to determine the observed climate statistics for the reference period (2001–2010). The statistics that are reproduced in the stochastic precipitation time series are the mean, variance, no-rain probability, skewness, and autocorrelation at daily scale. Disaggregation of daily to hourly precipitation is performed on the basis of empirical data. Air temperature is subdivided into a stochastic and a deterministic component. The temperature statistics of the deterministic part provided by the climate models are the monthly mean and the monthly standard deviation (SD). An autoregressive integrated moving average model is used for the stochastic generation of hourly air temperatures (50). The daily cycle is provided by historical data and is added to the stationary stochastic time series before destandardization with the monthly mean and SD. Differences between station observations and climate model outputs are first corrected through a nonlinear parametric bias correction method (51, 52). All climate statistics are evaluated separately for each month of the year and each decade from 2001 to 2100. Temperature lapse rates and precipitation gradients are used to distribute the downscaled climate data to every catchment grid cell and are estimated on the basis of historical station data, taking into account their spatial and temporal variability (13, 53). Daily cloud factors are sampled randomly from the available historical station data, differentiating between days with strong/medium/weak or no daily precipitation, and between spring–summer records and autumn–winter records to preserve the coupling of daily cloudiness with precipitation intensity. We force the model with 20 members of the stochastic input data ensemble generated for each GCM-RCP combination.

Model Calibration and Validation. The TOPKAPI-ETH setups used in this study have been established and thoroughly evaluated in three companion papers (12–14). Model parameters were calibrated with a multistep, multiobjective approach (12, 14). Carefully planned field data collection during two ablation seasons at both study sites constituted the basis for the setup and validation of the model (12, 14). For the purpose of preventing error compensation, each parameter was estimated on the basis of data that directly represent the corresponding physical process. A complete list of datasets and related model components and parameters is provided in *SI Appendix*, Table S1. Observed catchment runoff was used for model validation. In both regions, measured daily runoff from validation periods of 1–3 y could be reproduced by the model with a Nash–Sutcliffe efficiency (NSE) higher than 0.85 (*SI Appendix*, Table S3). In addition to the relatively short calibration and validation periods used in the companion papers (12–14), we use 9 y of available runoff data at either site to validate the seasonal runoff cycle as simulated by the stochastic runs for the reference period (*SI Appendix*, Fig. S4; NSE Juncal: 0.97; NSE Upper Langtang: 0.90).

Extreme Values Analysis. To assess possible changes in hydrological extremes, we look at the changes in different quantiles of annual runoff (*SI Appendix*, Figs. S8 and S9) and at the changes in the magnitude of annual peak daily runoff with different recurrence intervals (Fig. 5). Twenty stochastic realizations of each GCM-RCP combination lead to 200 annual values per decade that are used for this analysis.

Units of all water balance components in this study are expressed in millimeter water equivalents (volumes of water divided by catchment area). Details on the methodology and datasets can be found in *SI Appendix*.

ACKNOWLEDGMENTS. We are grateful to all the people who assisted with the data collection. We thank Andrés Rivera for providing data on the ice thickness of Juncal Norte Glacier and Thomas Mendlik for processing the CMIP5 model ensemble for the climate model selection. We are very grateful to the Hindu Kush Himalayan Cryosphere Monitoring Project implemented by the International Centre for Integrated Mountain Development and supported by the Norwegian Ministry of Foreign Affairs. Fieldwork was partially supported by the US Agency for International Development High Mountain Glacier Watershed Programs Climber–Scientist Grant CCRDCS0010. This study was supported by the Swiss National Science Foundation ("Understanding Contrasts in High Mountain Hydrology in Asia" project), with contributions from the Swiss State Secretariat for Education and Research (Grant CJRP-1003), the European Research Council under the European Union's Horizon 2020 Research and Innovation Program (Grant 676819) and the South Asia Research Hub of the UK Department for International Development.

1. Pellicciotti F, Bauder A, Parola M (2010) Effect of glaciers on streamflow trends in the Swiss Alps. *Water Resour Res* 46(10):W10522.
2. Bliss A, Hock R, Radić V (2014) Global response of glacier runoff to twenty-first century climate change. *J Geophys Res Earth Surf* 119(4):717–730.
3. Östrem G (1959) Ice melting under a thin layer of moraine, and the existence of ice cores in moraine ridges. *Geogr Ann* 41(4):228–230.
4. Benn D, Lehmkuhl F (2000) Mass balance and equilibrium-line altitudes of glaciers in high-mountain environments. *Quat Int* 65-66:15–29.
5. Harper JT, Humphrey NF (2003) High altitude Himalayan climate inferred from glacial ice flux. *Geophys Res Lett* 30(14):3–6.
6. Gabbi J, Huss M, Bauder A, Cao F, Schwikowski M (2015) The impact of Saharan dust and black carbon on albedo and long-term mass balance of an Alpine glacier. *Cryosphere* 9(4):1385–1400.
7. Fujita K (2008) Influence of precipitation seasonality on glacier mass balance and its sensitivity to climate change. *Ann Glaciol* 48(1):88–92.
8. Huss M, Hock R (2015) A new model for global glacier change and sea-level rise. *Front Earth Sci* 3(54):1–22.
9. Marzeion B, Jarosch H, Hofer M (2012) Past and future sea-level change from the surface mass balance of glaciers. *Cryosphere* 6(6):1295–1322.
10. Viviroli D, et al. (2011) Climate change and mountain water resources: Overview and recommendations for research, management and policy. *Hydrol Earth Syst Sci* 15(2):471–504.
11. Fernández A, Mark B (2016) Modeling modern glacier response to climate changes along the Andes Cordillera: A multiscale review. *J Adv Model Earth Syst* 8:467–495.
12. Ragettli S, et al. (2015) Unraveling the hydrology of a Himalayan catchment through integration of high resolution in situ data and remote sensing with an advanced simulation model. *Adv Water Resour* 78:94–111.
13. Ragettli S, Cortés G, McPhee J, Pellicciotti F (2014) An evaluation of approaches for modelling hydrological processes in high-elevation, glacierized Andean watersheds. *Hydrol Processes* 28(23):5674–5695.
14. Ragettli S, Pellicciotti F (2012) Calibration of a physically based, spatially distributed hydrological model in a glacierized basin: On the use of knowledge from glaciometeorological processes to constrain model parameters. *Water Resour Res* 48(3):W03509.
15. Ragettli S, Pellicciotti F, Bordoy R, Immerzeel WW (2013) Sources of uncertainty in modeling the glaciohydrological response of a Karakoram watershed to climate change. *Water Resour Res* 49(9):6048–6066.
16. Farinotti D (2013) On the effect of short-term climate variability on mountain glaciers: Insights from a case study. *J Glaciol* 59(217):992–1006.
17. Lutz A, Immerzeel W, Shrestha A, Bierkens M (2014) Consistent increase in High Asia's runoff due to increasing glacier melt and precipitation. *Nat Clim Chang* 4(7):587–592.
18. Fatichi S, Rimkus S, Burlando P, Bordoy R, Molnar P (2015) High-resolution distributed analysis of climate and anthropogenic changes on the hydrology of an Alpine catchment. *J Hydrol (Amst)* 525:362–382.
19. Pellicciotti F, Ragettli S, Carenzo M, McPhee J (2014) Changes of glaciers in the Andes of Chile and priorities for future work. *Sci Total Environ* 493:1197–1210.
20. Valdés-Pineda R, et al. (2014) Water governance in Chile: Availability, management and climate change. *J Hydrol (Amst)* 519:2538–2567.
21. Bown F, Rivera A, Acuña C (2008) Recent glacier variations at the Aconcagua basin, central Chilean Andes. *Ann Glaciol* 48(1):43–48.
22. Gascoin S, Lhermitte S, Kinnard C, Bortels K, Liston GE (2013) Wind effects on snow cover in Pascua-Lama, Dry Andes of Chile. *Adv Water Resour* 55:25–39.
23. Sharma B, et al. (2010) The Indus and the Ganges: River basins under extreme pressure. *Water Int* 35(5):493–521.
24. Rowan AV, Egholm DL, Quincey DJ, Glasser NF (2015) Modelling the feedbacks between mass balance, ice flow and debris transport to predict the response to climate change of debris-covered glaciers in the Himalaya. *Earth Planet Sci Lett* 430:427–438.
25. Scherler D, Bookhagen B, Strecker MR (2011) Spatially variable response of Himalayan glaciers to climate change affected by debris cover. *Nat Geosci* 4(3):156–159.
26. Kääb A, Berthier E, Nuth C, Gardelle J, Arnaud Y (2012) Contrasting patterns of early twenty-first-century glacier mass change in the Himalayas. *Nature* 488(7412):495–498.
27. Miles ES, et al. (2016) Refined energy-balance modelling of a supraglacial pond, Langtang Khola, Nepal. *Ann Glaciol* 57(71):29–40.
28. Buri P, Pellicciotti F, Steiner JF, Miles ES, Immerzeel WW (2016) A grid-based model of backwasting of supraglacial ice cliffs on debris-covered glaciers. *Ann Glaciol* 57(71):199–211.
29. Benn DI, et al. (2012) Response of debris-covered glaciers in the Mount Everest region to recent warming, and implications for outburst flood hazards. *Earth Sci Rev* 114(1-2):156–174.
30. Immerzeel WW, Pellicciotti F, Bierkens MFP (2013) Rising river flows throughout the twenty-first century in two Himalayan glacierized watersheds. *Nat Geosci* 6(8):742–745.
31. Kaser G, Grosshauser M, Marzeion B (2010) Contribution potential of glaciers to water availability in different climate regimes. *Proc Natl Acad Sci USA* 107(47):20223–20227.
32. Norris J, Carvalho L (2015) WRF simulations of two extreme snowfall events associated with contrasting extratropical cyclones over the western and central Himalaya. *J Geophys Res Atmos* 120(8):1–25.
33. Collier E, Immerzeel W (2015) High-resolution modeling of atmospheric dynamics in the Nepalese Himalaya. *J Geophys Res Atmos* 120(19):9882–9896.
34. Lafon T, Dadson S, Buys G, Prudhomme C (2013) Bias correction of daily precipitation simulated by a regional climate model: A comparison of methods. *Int J Climatol* 33(6):1367–1381.
35. Gabbi J, Carenzo M, Pellicciotti F, Bauder A, Funk M (2014) A comparison of empirical and physically-based glacier surface melt models for long-term simulations of glacier response. *J Glaciol* 60(224):1140–1154.
36. Immerzeel WW, van Beek LP, Konz M, Shrestha AB, Bierkens MFP (2012) Hydrological response to climate change in a glacierized catchment in the Himalayas. *Clim Change* 110(3-4):721–736.
37. Beven K (2006) A manifesto for the equifinality thesis. *J Hydrol* 320(1-2):18–36.
38. Shea JM, Immerzeel WW, Wagnon P, Vincent C, Bajracharya S (2015) Modelling glacier change in the Everest region, Nepal Himalaya. *Cryosphere* 9(3):1105–1128.
39. Fujita K, Sakai A (2014) Modelling runoff from a Himalayan debris-covered glacier. *Hydrol Earth Syst Sci* 18(7):2679–2694.
40. Fatichi S, et al. (2016) An overview of current applications, challenges, and future trends in distributed process-based models in hydrology. *J Hydrol (Amst)* 537:45–60.
41. Pellicciotti F, et al. (2005) An enhanced temperature-index glacier melt model including the shortwave radiation balance: Development and testing for Haut Glacier d'Arolla, Switzerland. *J Glaciol* 51(175):573–587.
42. Brock B, Willis I, Sharp M (2000) Measurement and parameterization of albedo variations at Haut Glacier d'Arolla, Switzerland. *J Glaciol* 46(155):675–688.
43. Reid TD, Brock BW (2010) An energy-balance model for debris-covered glaciers including heat conduction through the debris layer. *J Glaciol* 56(199):903–916.
44. Immerzeel WW, et al. (2014) High-resolution monitoring of Himalayan glacier dynamics using unmanned aerial vehicles. *Remote Sens Environ* 150:93–103.
45. Ragettli S, Bolch T, Pellicciotti F (2016) Heterogeneous glacier thinning patterns over the last 40 years in Langtang Himal. *Cryosph Discuss* 2016:1–53.
46. Bernhardt M, Schulz K (2010) SnowSlide: A simple routine for calculating gravitational snow transport. *Geophys Res Lett* 37(11):L11502.
47. Huss M, Jouvet G, Farinotti D, Bauder A (2010) Future high-mountain hydrology: A new parameterization of glacier retreat. *Hydrol Earth Syst Sci* 14(5):815–829.
48. Frey H, et al. (2014) Estimating the volume of glaciers in the Himalayan–Karakoram region using different methods. *Cryosphere* 8(6):2313–2333.
49. Ciarapica L, Todini E (2002) TOPKAPI: A model for the representation of the rainfall-runoff process at different scales. *Hydrol Processes* 16(2):207–229.
50. Box G, Jenkins G, Reinsel G (2008) *Time Series Analysis: Forecasting and Control* (Wiley, Hoboken, NJ), 4th Ed.
51. Leander R, Buishand TA (2007) Resampling of regional climate model output for the simulation of extreme river flows. *J Hydrol (Amst)* 332(3-4):487–496.
52. Bordoy R, Burlando P (2013) Bias correction of regional climate model simulations in a region of complex orography. *J Appl Meteorol Climatol* 52(1):82–101.
53. Immerzeel WW, Petersen L, Ragettli S, Pellicciotti F (2014) The importance of observed gradients of air temperature and precipitation for modeling runoff from a glacierized watershed in the Nepalese Himalayas. *Water Resour Res* 50(3):2212–2226.